



EXPERIMENTAL INVESTIGATION OF THE USE OF WIND ROTOR
AS A POWER GENERATING DEVICE FROM SMALL RIVERS
(Part 1).

N. SH. MATTA*

ABSTRACT

This work describes model tests performed on vertical axis wind buckets. A possible application of this wind rotor would be used to extract energy from slow moving water (no head streams) through small rivers. The major use of the design proposed is to provide small amounts of electric power for areas far from the main electric power systems especially for developing countries. The test model has been designed and aerodynamically tested for different wind bucket geometries.

* Lecturer, Mechanical Engineering & Energy Department
Faculty of Engineering & Technology. Minia University
Minia - Egypt

INTRODUCTION

As reported by ref. [1] Microhydro is defined as having a generating capacity of up to about 15 kilowatts. It can provide basic lighting and other services to a village in a developed country. Microhydro generation is best suited to providing small amounts of power to individual houses, farms in an isolated areas. This plants use much simpler and lower cost technology than minihydro plants. For this resion, microhydro plants are usually will suited to village level development and local self-help projects . Units can be built by people without much special training, using mostly local materials and skills. They are usually lower in cost than minihydro and conventional hydro plants, but they are also less efficient, and the quality of the electricity is not as good. They may be used also in grinding grain or pumping water. For the electrical gear, the system needs an alternator which produces low-voltage AC. This power goes through a rectifier and voltage regulator which convert it to DC, which is then either used directly, or used to charge batteries if more power is being produced than is needed. The batteries return the power later when more power is being used than produced. The system may be connected to an inverter , which converts the low-voltage DC power from the batteries to AC, for use with appliances requiring AC power.

For small head of water exists, a number of types of water turbines are available for extracting power from the hydro sources. All of these work by the converting the pressure head to kinetic energy involving relatively high velocities. If the source is a river having a negligible head, the type of turbine required is one which will extract energy directly from a slow-moving stream: The turbine must be relatively simple and cheap to make, and must be efficient. The ancient paddle wheel and the under-shot water wheel both suffered the disadvantage that they were inefficient and required the use of a lot of material in their construction. The need to seek more efficient alternatives.

The well known principle of the vertical axis turbine has been applied in such machinery as: the Darrieus wind turbine for extracting energy from small rivers or canals current for water pumping and/or electricity generation. By means of pulleys, belts and a gear box, the speed can be increased to the alternatur speed range. Boissevain (1971) designed a horizontal axis propeller turbine attached to a float and the float was anchored to the river bottom [2]. NRC (Canada) designed a vertical axis water turbine with 2.4 m rotor diameter (aerofoil blades shape) 10kw output [3].

The aim of the present study is to introduce a possible design for a vertical axis water turbine with a bucketed rotor. A bridge-type plate form mounted across two floating pontoons made from wood and oil drums, must be used. The designated vertical axis water turbine would be mounted at the centre of the of the bridge structure. The whole assembly could be located in the desired position in the river and fixed by chain or ropes.

This work concentrated to give some lights about the rotor characteristics experimentally. The test rig has been assembled at the hydraulic laboratory of Minia Faculty of Engineering and Technology. Different shapes of buckets were tried, each attempting to enhance the rotor performance.

EXPERIMENTAL ARRANGEMENTS:

Experimental Method:

The experiments were conducted in a low speed wind tunnel for different shapes of bucketed rotors. Models were tested at Reynolds number 12×10^4 , in terms of the rotor radius, to simulate the conditions of the proposed prototype. The test rig is shown in Fig. 1. During the tests, each model was mounted with the main shaft. A rope was rapped around the pulley. One end of the rope was attached to a fixed lever and the other end was attached to the weight holder (Fig. 1). Measurements include rotor rotational speed, free stream velocity and rotor output torque. The data is presented in the usual form of the power coefficient C_p which defined as:

$$C_p = \frac{T \cdot \omega}{0.5 \rho \cdot (V - u)^2 \cdot u \cdot A}$$

as function of the tip-speed ratio, (TSR).

Test Models:

The different types of the tested models are shown in Fig. 2. The different models were made and tested to predict the best geometry of the buckets.

DISCUSSION OF RESULTS AND CONCLUSION

The rotor power coefficient vs. tip-speed ratio for the different configurations of the rotors are shown in Fig. 3. Comparison between the rotors characteristics are shown in Fig. 4. The average value of power coefficient, C_p , for two blade rotor (model 1) is about 0.07 for TSR range of 0.03 : 0.06. If the same blades are shrouded as indicated in model 2, the average value of C_p will increase to 0.09 and TSR range will increase also to 0.035 : 0.08. Comparison between test models 1, 6 and 11 shows that the average value of C_p increased according to increasing the number of blades which reaches 0.13 for 3 blades, 0.18 for 4 blades. Model 10 is the same model 6 but its blades are shrouded. The average value of C_p and the TSR rate are increased to 0.15, 0.03 : 0.095. Comparison between models 3, 5, and 7 gives the same trend. For 4 buckets the average C_p reaches 0.2 for TSR range 0.055 : 0.098. Prism shape model gives better results than the semi circular for the same swept area as shown from the values of models 7, 13. The average value of C_p reaches 0.25 for TSR range 0.05 : 0.10.

For the semi elliptic -double buckets(Model 8),wide range of TSR is obtained(0.08 : 0.13)when compared with Savonius model (Test model 9). Comparison between models 12,14 for the semi-elliptic rotors indicates that increasing the bucket opening (for the same bucket dimension),increase C_p to average value of 0.25 for TSR range 0.05 : 0.12.

Therefore,models 8,13,and 14 are recommended for the proposed system. As a conclusion , the efficiency of the turbine rotor remain low, of the order of 20%. During preparing this paper, some modifications are studied experimentally to refine the design of the models 8,13 and 14. Few percentage points may be gained for rotor power coefficient.

REFERENCES

1. Christopher S. Weaver, " Understanding Micro-hydro-electric Generation", VITA Tech. Paper TP 18:01/ 85 (1985).
2. Mathew G. Boissevain, VITA Technical Bulletins, ISBN 0-86619-079-1, 51001-BK,(1979).
3. Barry V. Davis, " Modern Power Systems",pp. 29-34, February 1983.

NOMENCLATURE

- A = Rotor swept area
- C_p = Rotor power coefficient
- T = Torque
- TSR= Tip speed ratio= u/V
- u = Rotor tip speed
- V = Free stream velocity
- = Rotor angular velocity
- = Air density

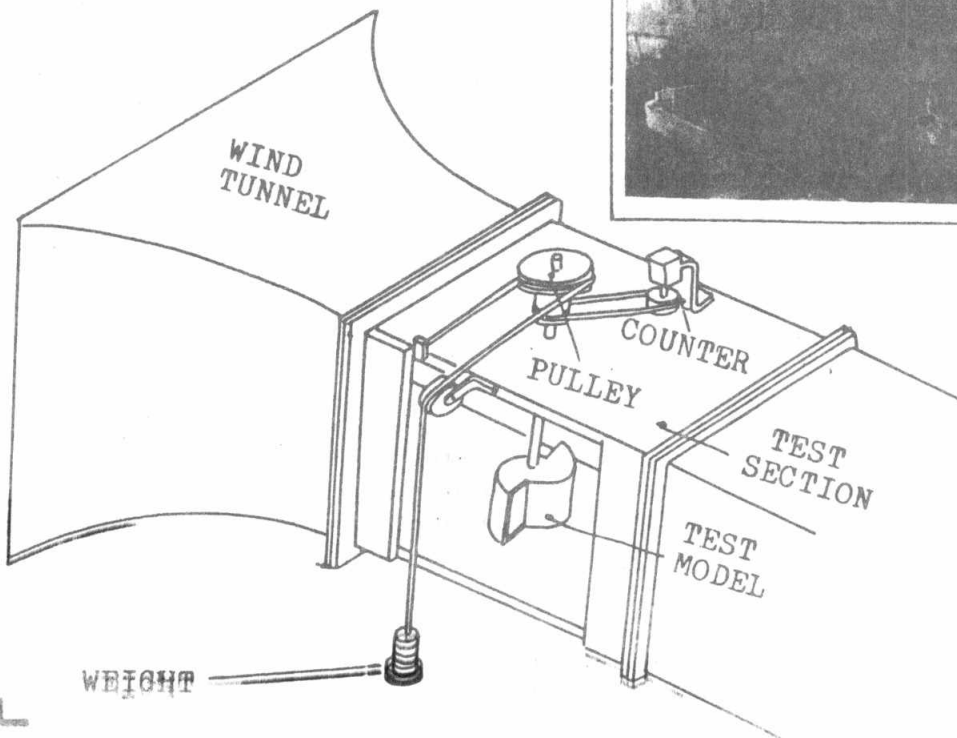
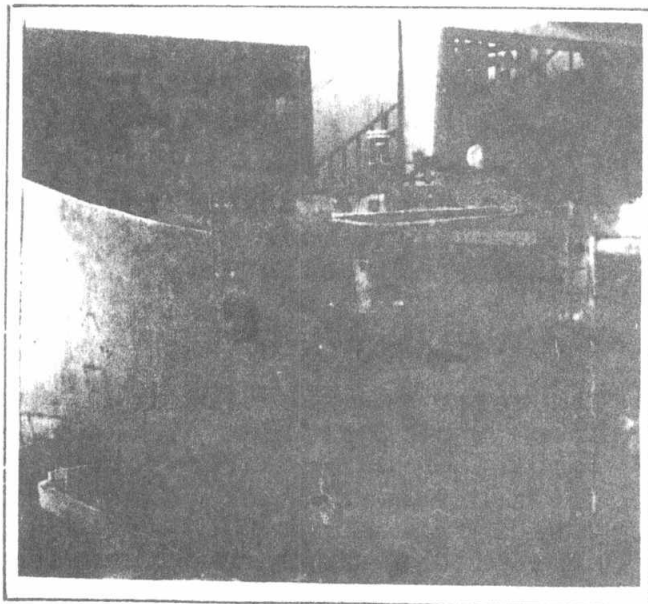


Fig. 1
Test Rig.

EN-4	453
------	-----

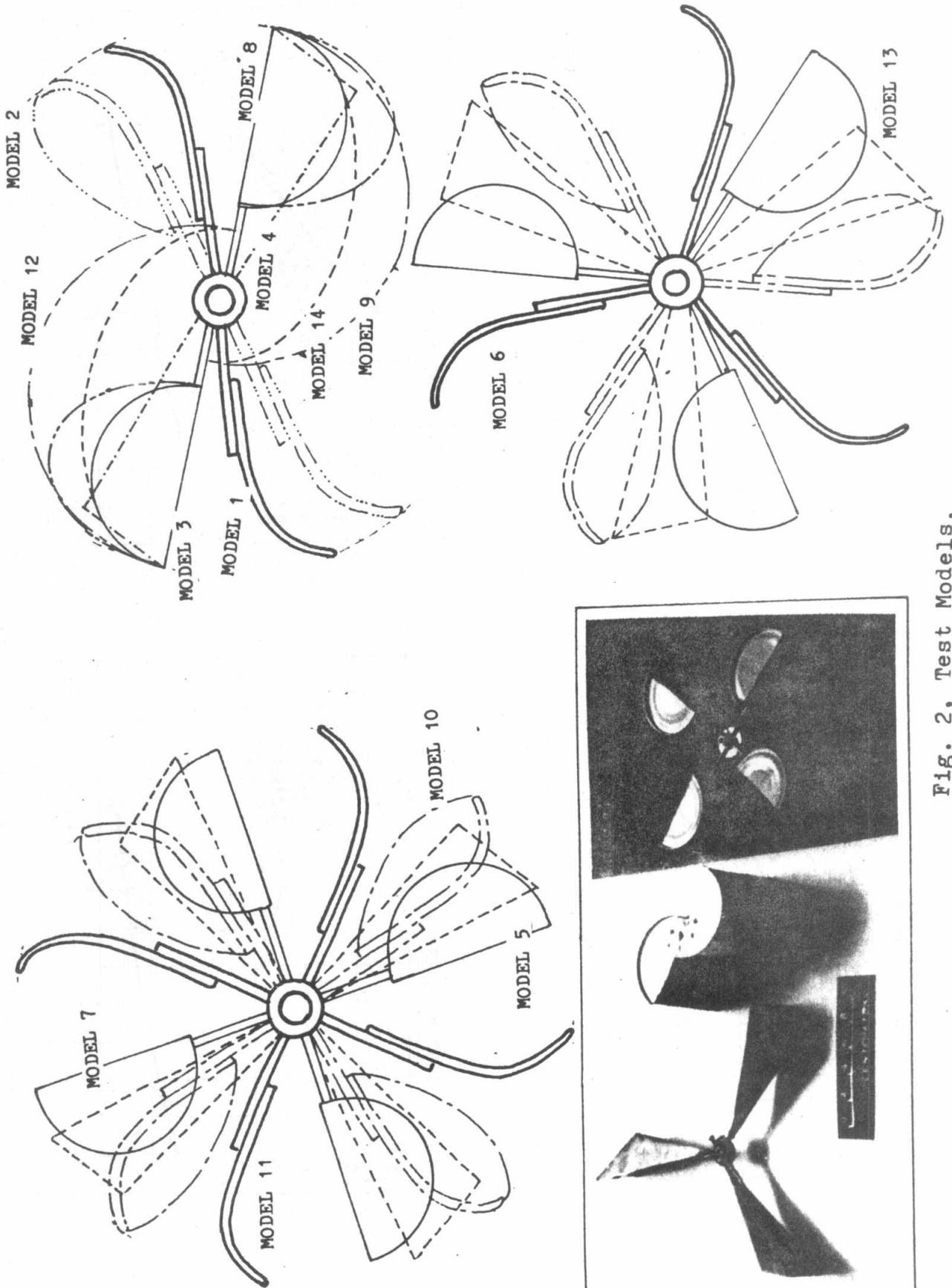


Fig. 2, Test Models.

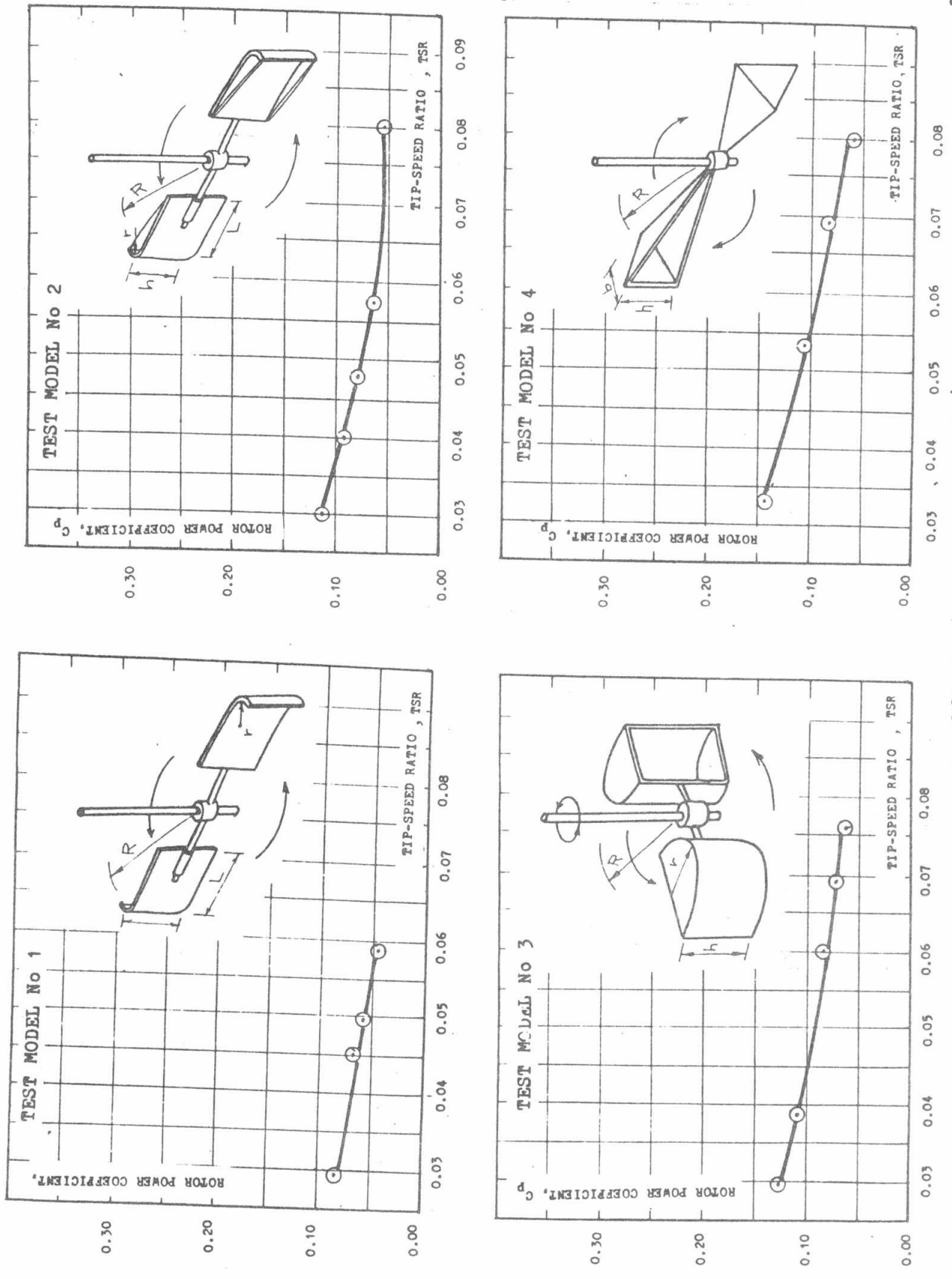


Fig. 3, Rotor Power Coefficient vs. Tip Speed Ratio.

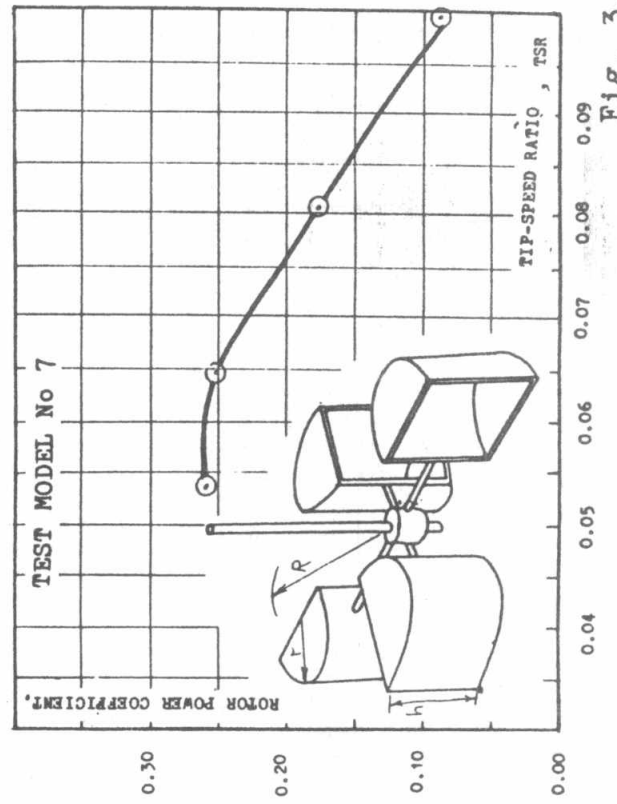
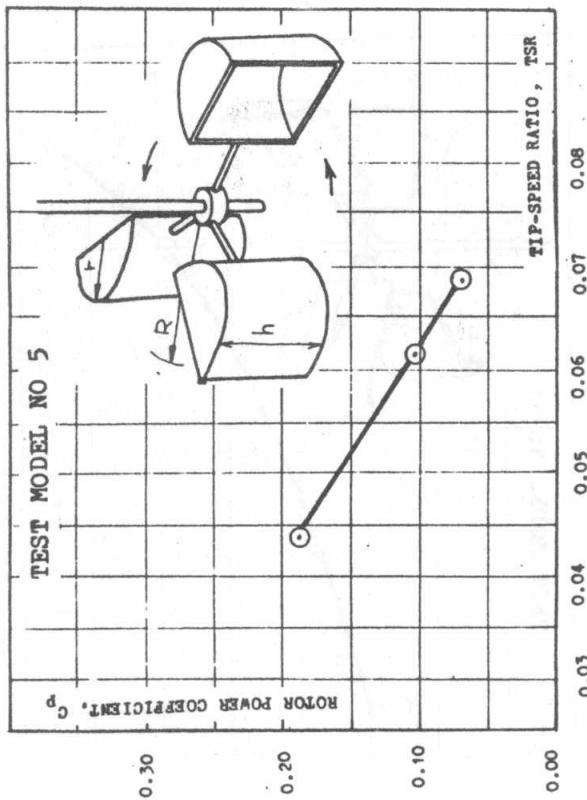
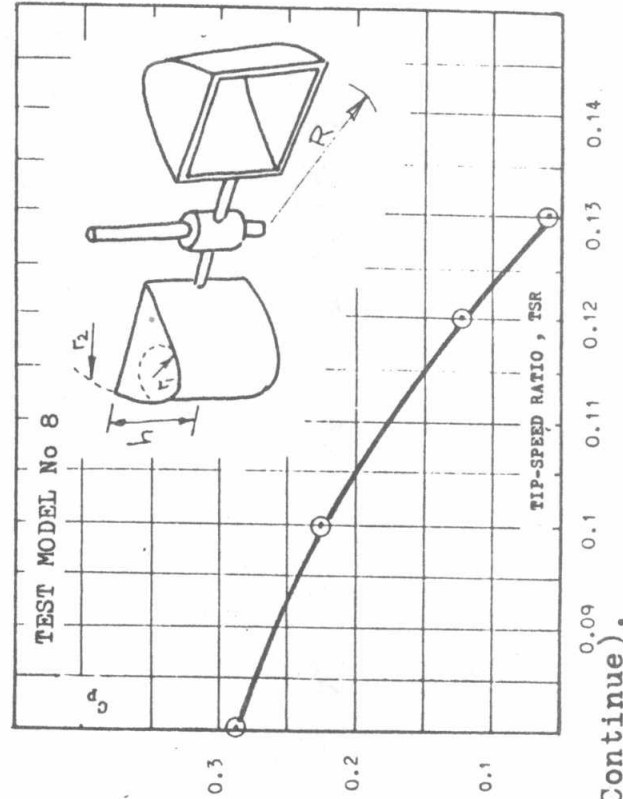
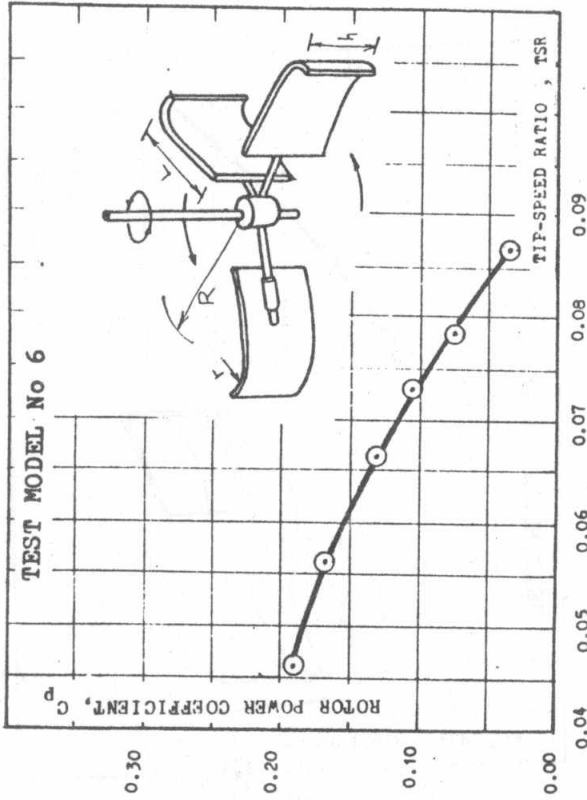


Fig. 3, (Continue).

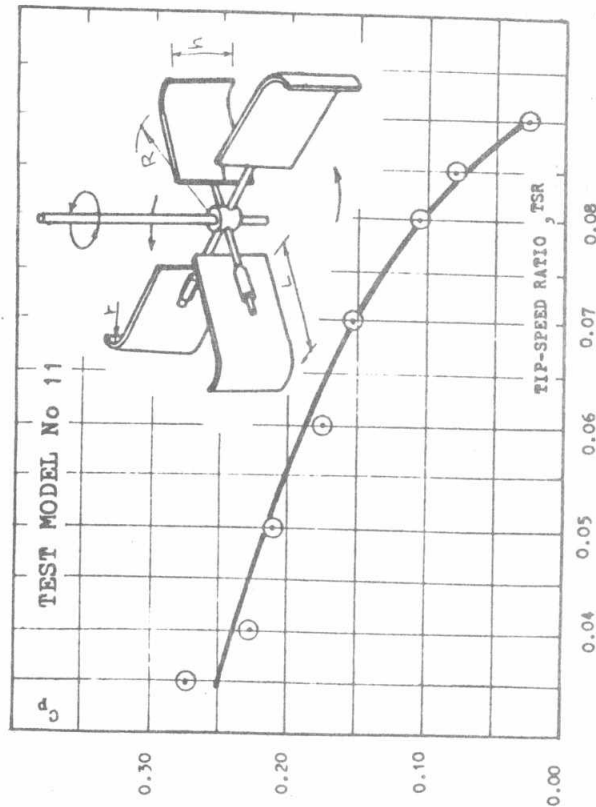
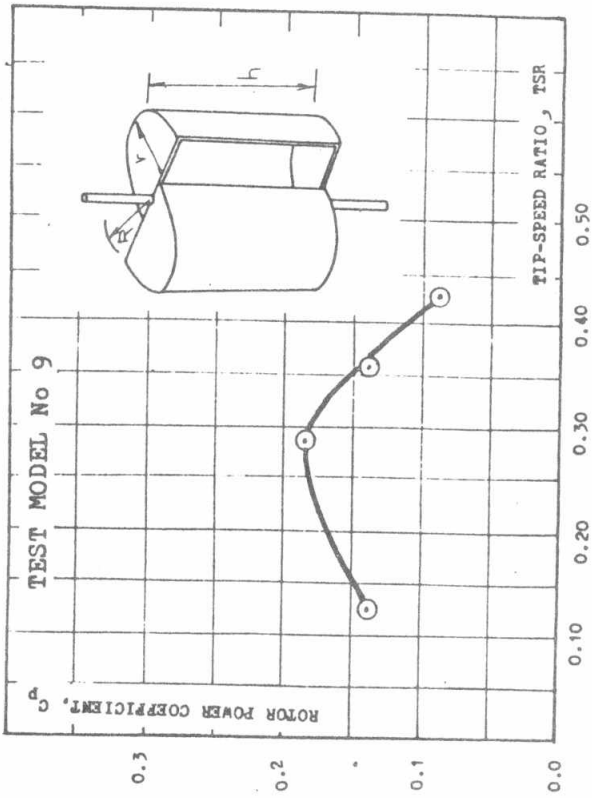
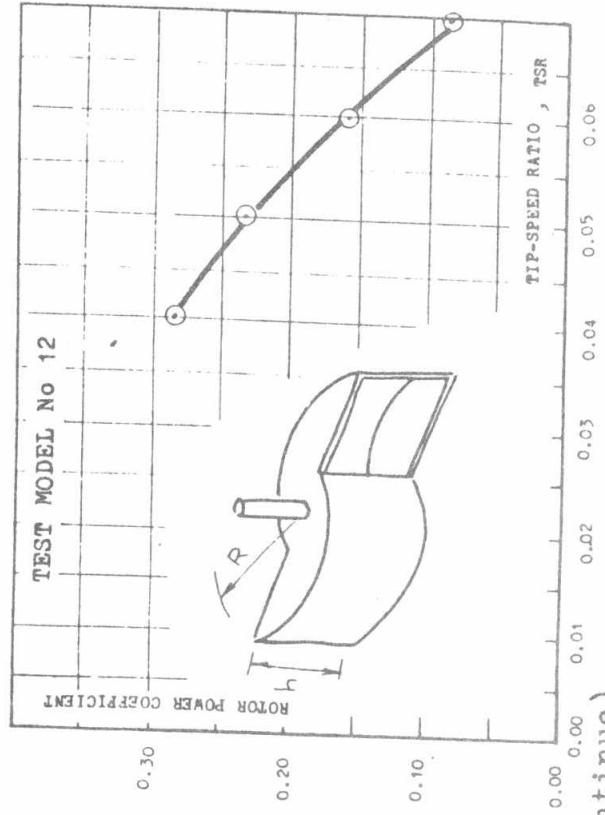
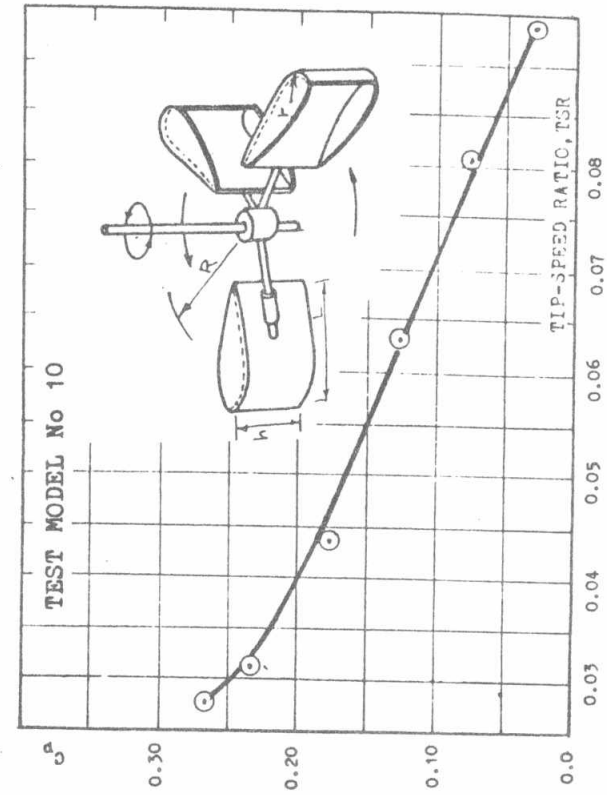


Fig. 3, (Continue).

6

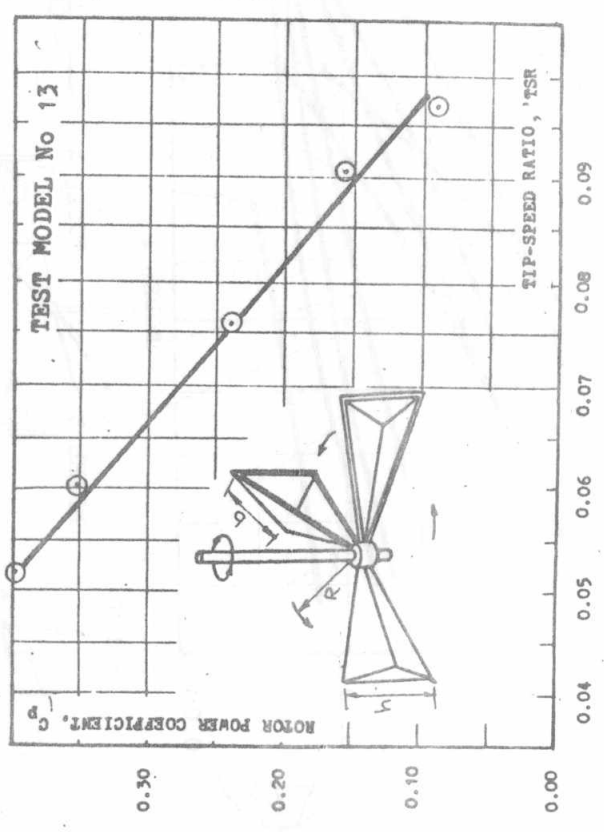
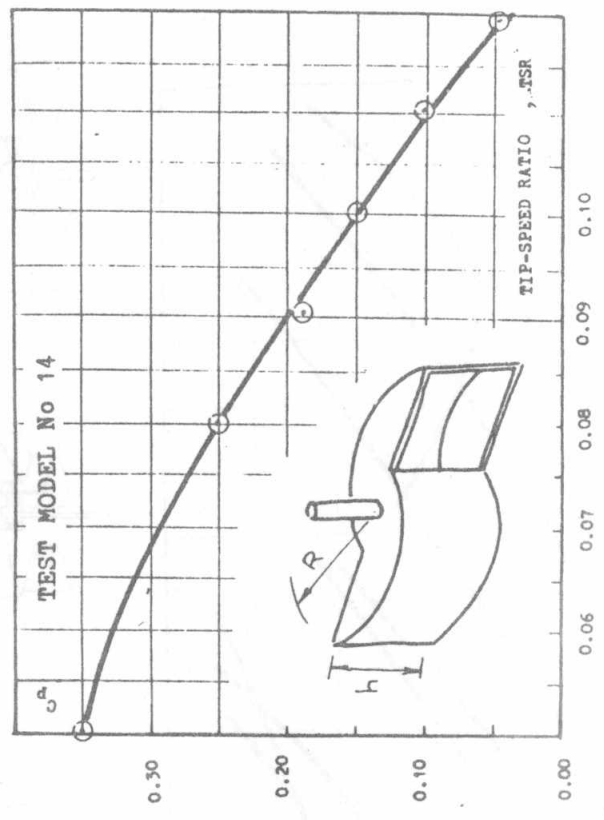


Fig. 3, (Continue)

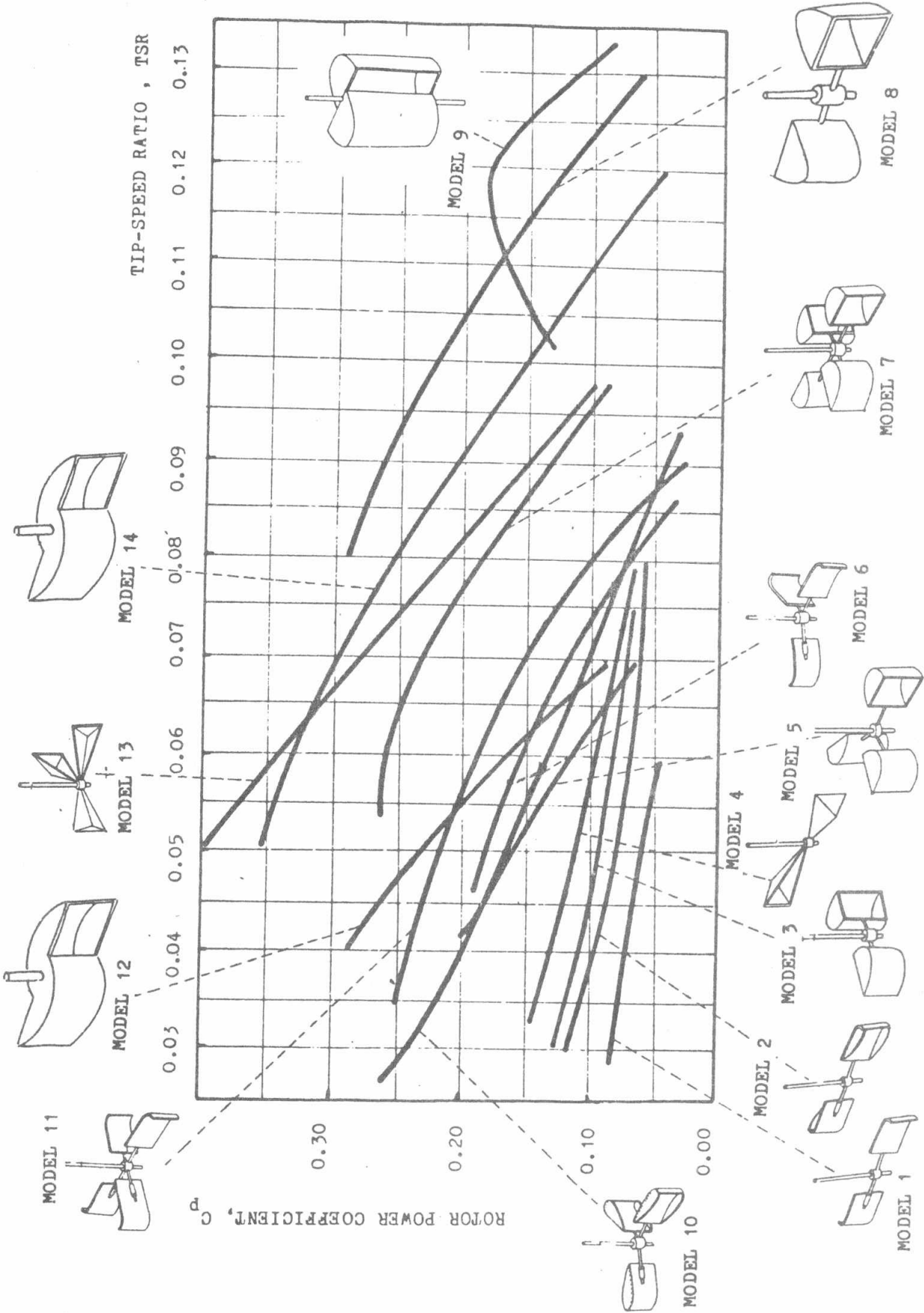


FIG. 4. Comparison Between Different Power Coefficients.



SPECTRAL RESPONSE IN POLYCRYSTALLINE

SILICON SOLAR CELLS

S. Elewa, M. El-Koosy*, A.Zekry, H.F.Ragai and N.Saleh.

ABSTRACT

A theoretical model has been introduced for the calculation of the collection efficiency (spectral response) in polycrystalline silicon solar cells. The contributions from emitter, base and depletion layer are taken into consideration. The effect of the grain size and the effect of the drift field in the emitter or the base region are examined. It is found that the dominant mechanism of photogenerated carrier collection at small grain sizes ($10 \mu\text{m}$ or less) is the built in field collection, whereas at higher grain sizes ($100 \mu\text{m}$ or more), the collection is dominated by carrier diffusion towards the junction.

Faculty of eng. Ain Shams university.
* Armament Authority, Kobri El Koba, Cairo.

INTRODUCTION

The interest in polycrystalline silicon has increased recently because of its potential in the fabrication of inexpensive solar cells , however these solar cells have low efficiency due to the recombination of photogenerated carriers at the grain boundaries.

The cell performance is affected strongly by the grain size which is in fact the major mechanism in the performance .

In this work, the effect of the grain size on the spectral response is examined, further more, the effect of an electric field is examined too.

THE PHYSICAL MODEL AND THE NUMERICAL CALCULATIONS

The geometry of the grain, its symmetry axis, and the coordinate system to be used are shown in fig.1 , it is assumed that the poly. silicon layer is composed of columnar grains , for the purpose of calculations, the grains are idealized to right circular cylinders. Inside the grain, the material is assumed to be uniform so that symmetry exists about the X axis, thereby reducing the system to 2 independent coordinate variables.

For the implementation of the numerical simulation, the grain (except for the depletion layer) is divided into 6 and 100 parts in the X direction for the emitter and base region respectively. The large number of divisions in the X direction is dictated by the rapid change in the carrier concentration caused by the high absorption coefficient , for the radial direction, the grain is divided into 3 parts for the emitter region and 4 parts in the base region (since only diffusion limits the rate of density change in this direction), see fig.2 . For each elemental volume formed by the grids, the steady state continuity equation under optical illumination is solved in cylindrical coordinates.

The continuity equation can be written as :

$$-D_m \left(\frac{\partial^2 m}{\partial x^2} \right) - D_m \left(\frac{\partial^2 m}{\partial r^2} \right) + \mu_m E_m \left(\frac{\partial m}{\partial x} \right) + \left(\mu_m E_m - D_m / r \right) \left(\frac{\partial m}{\partial r} \right) + \left(\frac{1}{r} \right) \mu_m E_m m = G(\lambda, x) + m / \tau_m \quad (1)$$

Where:

D_m is the diffusion constant for the minority carriers

m is the density of excess (photogenerated) minority carriers

- τ_m is the minority carrier recombination time constant .
- G..... is the generation rate of minority carriers .
- E..... is the drift field in the given direction

The generation rate for each volume is determined by dividing the AMO spectral response to 15 packets of 0.5 μm width , using the appropriate coefficient for each center wavelength , the generation due to each wavelength packet is assumed at each position along the axis.

The excess minority carrier density is assumed to be reduced to zero at the back due to the ohmic contact and to zero at the depletion layer edges due to the barrier electric field . It is also assumed that all carriers generated within the depletion layer are collected due to the high electric field in this region and the low carrier concentration through bulk recombination centers or through grain boundary states.

The continuity equation [1-2] is solved numerically using the finite - difference method [3], the system of linear equations obtained by the finite-difference method at the different grid points is solved numerically using Gauss-Jordan elimination method [4]. In this way the minority carrier concentration in each volume is determined using the following boundary conditions [5]

1-For the surface
$$-D_0 \frac{\partial P_n}{\partial x} + \mu_p E_x P_n = -S (P_n - P_{n0}) \quad (2)$$

2- For the emitter grain boundary
$$-D \frac{\partial P_n}{\partial r} + \mu_p E_r P_n = -S (P_n - P_{n0}) \quad (3)$$

3- For the grain center (emitter)
$$-D \frac{\partial P_n}{\partial r} + \mu_p E_r P_n = 0 \quad (4)$$

4- For the emitter junction
$$P_n = P_{n0} \quad (5)$$

5- For the base grain boundary
$$-D \frac{\partial n_p}{\partial r} - \mu_n E_r n_p = S (n_p - n_{p0}) \quad (6)$$

6- For the base grain center
$$-D \frac{\partial n_p}{\partial r} - \mu_n E_r n_p = 0 \quad (7)$$

7- For the base junction
$$n_p = n_{p0} \quad (8)$$

8- For the ohmic contact
$$n_p = n_{p0} \quad (9)$$

The gradient of the minority carrier concentration computed at the depletion layer edge is then used to compute the photo current components for each wavelength packet.

The data used in our calculations are [5-6]:

a) For the top region;

$$N_D = 5 \times 10^{19} / \text{cm}^3$$

$$D_p = 1.295 \text{ cm}^2 / \text{s}$$

$$\tau_p = 2.5 \times 10^{-6} \text{ s}$$

b) For the base region;

$$N_A = 5 \times 10^{17} / \text{cm}^3$$

$$D_n = 27 \text{ cm}^2 / \text{s}$$

$$\tau_n = 0.5 \times 10^{-6} \text{ s}$$

NUMERICAL CALCULATION OF THE SPECTRAL RESPONSE

Definition

The photocurrent collected at each wavelength relative to the number of photons incident on the surface at that wavelength determines the spectral response of the device . The internal spectral response is defined as the number of electron - hole pairs collected under short circuit condition relative to the number of photons entering the material.

The internal spectral response can be expressed as [1] ;

$$SR = \frac{J_E(\lambda)}{q\Phi(\lambda)[1-R(\lambda)]} + \frac{J_B(\lambda)}{q\Phi(\lambda)[1-R(\lambda)]} + \frac{J_{dr}(\lambda)}{q\Phi(\lambda)[1-R(\lambda)]} \quad (10)$$

Where;

$J_E(\lambda)$ is the short circuit current density due to the emitter region at wavelength λ .

$J_B(\lambda)$ is the short circuit current density due to the base region at wavelength λ .

$J_{dr}(\lambda)$ is the short circuit current density due to the depletion region at wavelength λ .

$\Phi(\lambda)$ is the incident photon normal to the surface at wavelength λ .

$R(\lambda)$ is the reflected part at the surface at wavelength λ .

RESULTS AND DISCUSSION

Fig.4 shows the 3 components of the calculated spectral response (the diffused top region ,the depletion region and base region).It is clear from the figure that the base component dominates at long wavelengths where most of carriers are generated in this region due to the low absorption coefficients. The contribution from the emitter region

is enhanced in the short wavelength region where most of the photons are absorbed near the surface . The contribution from the depletion layer is considerable only in the range from $0.4 \mu\text{m}$ to $0.6 \mu\text{m}$, this contribution will not exceed that from the diffused layer below $0.4 \mu\text{m}$ under any practical conditions due to the very high absorption coefficient of silicon below $0.4 \mu\text{m}$ which causes almost all the light to be absorbed in the first 1000 \AA next to the cell surface.

The high value of the absorption coefficient for silicon in the small wavelengths is responsible also for high spectral response value in the range from 0.4 to $0.5 \mu\text{m}$. The decreasing of the SR values with increasing λ in this range is mainly due to the decrease in the absorption coefficient and the absence of an effective base contribution . For higher wavelengths, the base contribution begins to play the main role in the spectral response and the curve starts to increase again rapidly due to the base contribution , see fig. 3.

EFFECT OF GRAIN SIZE ON THE SPECTRAL RESPONSE

Fig. 4 shows the variations of the spectral response as a function of the wavelength (λ) for different grain size. It is clear from the curve that for small grain sizes ($10 \mu\text{m}$) the spectral response is maximum near a wavelength equals $0.4 \mu\text{m}$. The decrease observed in the spectral response with increasing the wavelength is due to the fact that the probability of the carriers generated away from the junction by long wavelength photons decrease exponentially to zero.

With increasing the grain size, the diffusion length increases and the probability of collection of minority carriers generated away from the junction increases also. The peak point is shifted towards longer wavelengths as the grain size increases due to the same reason while no difference is observed in the short wavelengths due to the absorption of photons in this range at the surface close to the junction.

CONCLUSION

The performance of polycrystalline silicon solar cell is greatly related to the average grain size for the used polycrystalline silicon wafer . The computations showed that SR enhances with the increase in grain size. An improvement in the collection efficiency can be attained also by an electric field in the emitter region or the base or both

REFERENCES

- 1-Hovel,H.J., Semiconductor and semimetals , Vol. 11, Academic Press, New York,(1975).
- 2-El Nahawy,s and Adeeb,N., Thin film polycrystalline silicon P/N junction solar cells with preferential doping, Solid State Electronics, Vol.25,No. 11, (1977).
- 3-Smith,G.D., Numerical Solution Of Partial Differential Equations,Clarendon Press,Oxford,(1978).
- 4-Hoenbeck,R.W., Numerical Methods , Quantum Publishers Inc.,New York , (1975).
- 5-Holder,N.J., Grain Boundary Effects In Polycrystalline Silicon Solar Cells, Solar Cell,No. 8,(1983).
- 6-Lanza,C., Efficiency Calculations For Thin Film Polycrystalline Semiconductor P/N Junction Solar Cell ,IEEE,Vol.,ED-27,No.11,(1980).

6

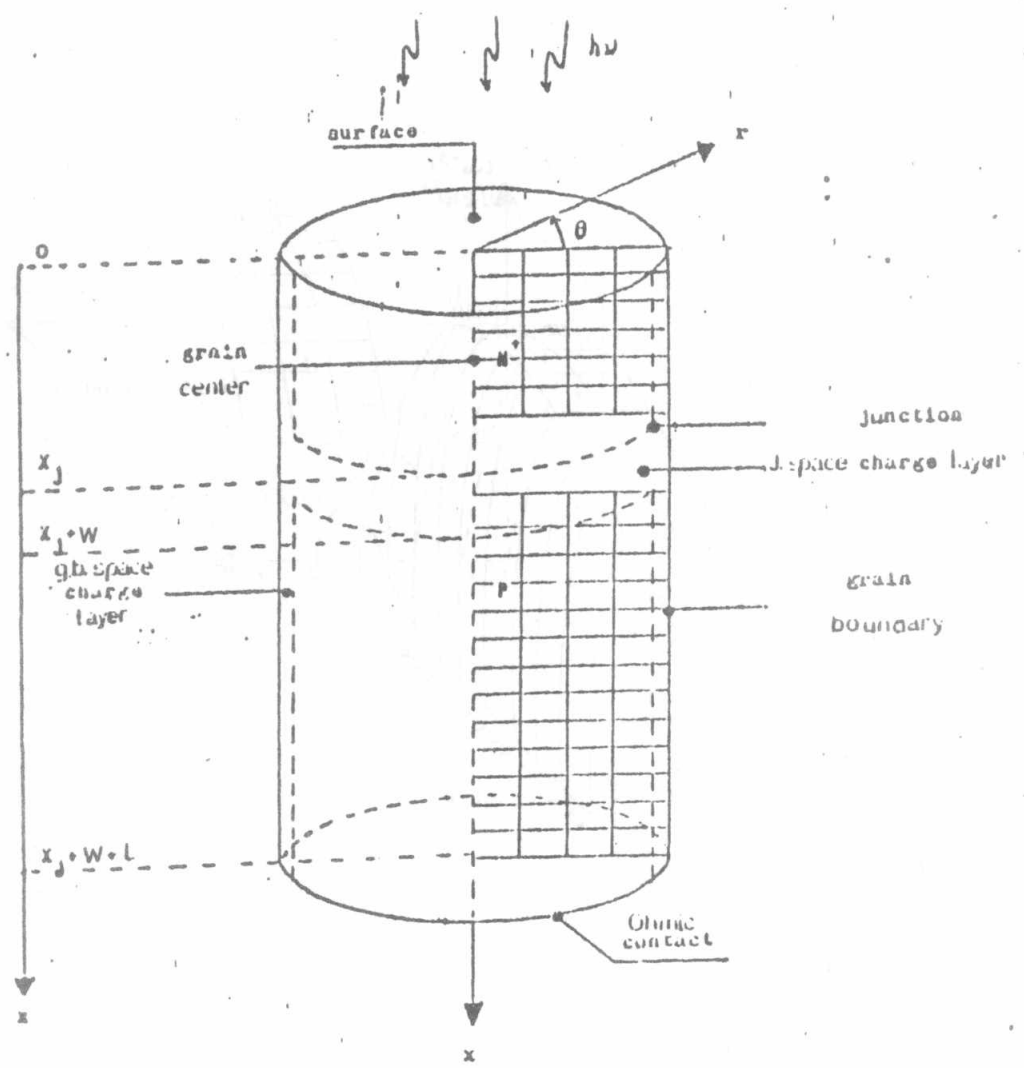


Fig. 1. Grain geometry used in the numerical calculations

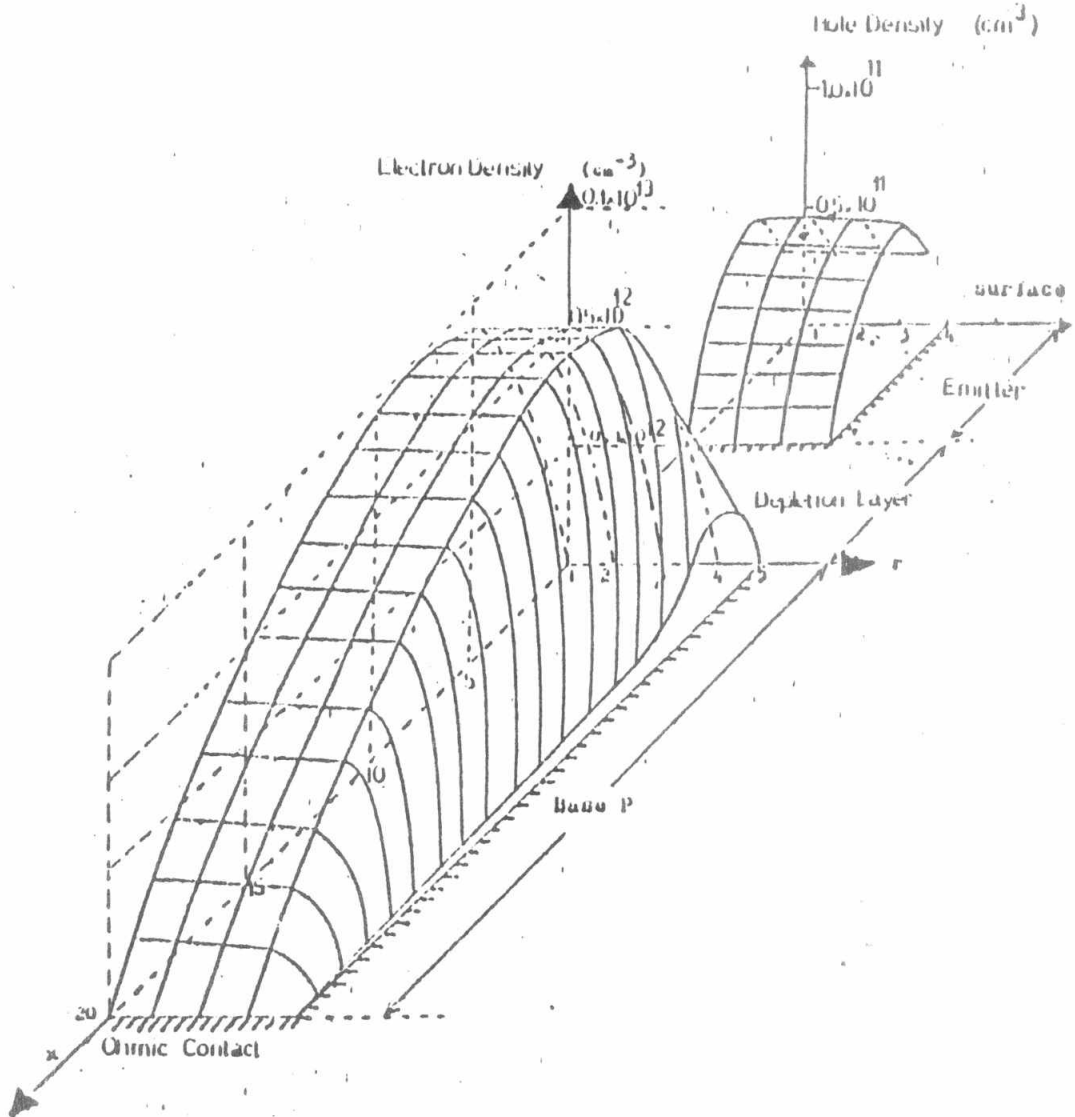


Fig. 2 . Volume representation of the density of minority carriers in the base and emitter for a cylindrical grain of polycrystalline silicon solar cell.

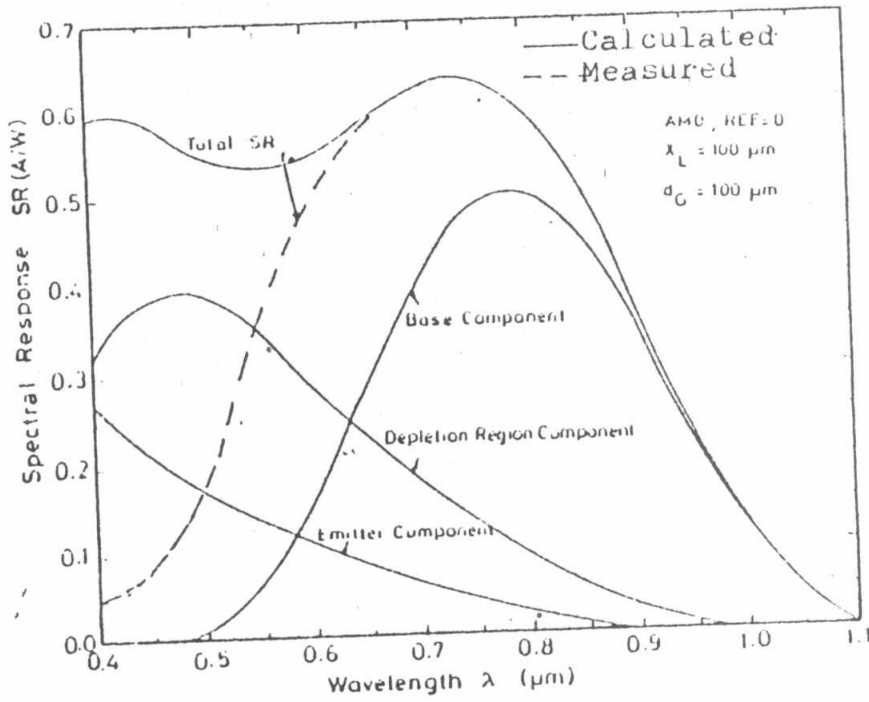


Fig. 3 Total Spectral Response and its Individuals

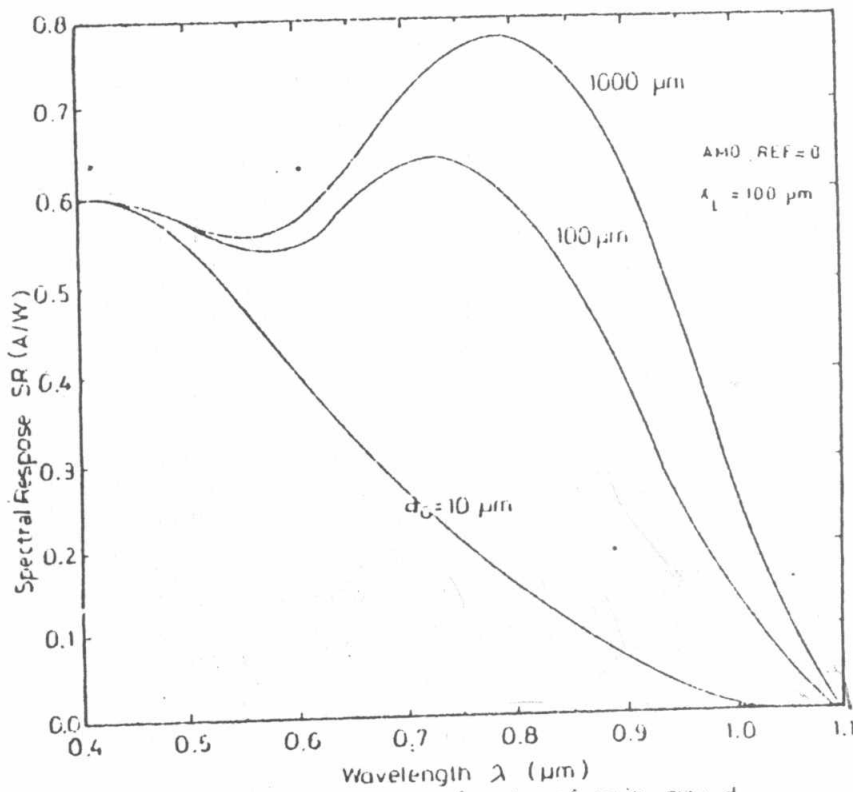


Fig. 4 Spectral response as a function of grain size d_G